Omnithermal Restructurable Metasurfaces for Both Infrared-Light Illusion and Visible-Light Similarity

Jun Wang, Fubao Yang, Liujun Xu, and Jiping Huang[*]

Department of Physics, State Key Laboratory of Surface Physics, and Key Laboratory of Micro and Nano Photonic Structures (MOE), Fudan University, 200438 Shanghai, China

The existing challenges in designing infrared illusion are related to complex working environments, multifold heat-transfer modes, and fabrication difficulties. Recent research focuses mainly on solving one of these challenges. In this work, we consider them synthetically and propose a class of restructurable metasurfaces to show both illusion viewed in infrared light and similarity in when viewed in visible light. We consider the three basic modes of heat transfer (omnithermotics) in theoretical designs and use radiation-cavity effects in experimental manufacture. We also make it feasible to tune the surface temperature and emissivity synergistically. Besides, such metasurfaces can work in temperature-varying backgrounds and transient states. This scheme may not only provide a platform for the design of adaptable thermal illusion but may also show robustness under multifrequency detection.

I. INTRODUCTION

The temperature signals of macroscopic objects can be observed by infrared imaging because all objects with nonzero temperatures emit electromagnetic energy, which is known as thermal radiation [1–3]. The Wien law [4] implies that within a large temperature range (1–1000 K), the radiation-spectrum peak of an ideal black body is located in the infrared region. This intrinsic property is extensively applied in industry, military detection, and daily life. Naturally, the technology of thermal illusion [5–9] has attracted much attention due to its promising prospects in illusion or camouflage; namely, misleading or camouflaged thermal signals. The former ("illusion") means that an existing object exists in infrared imaging, replacing another nonexisting object [5–7]. In contrast, the latter ("camouflage") means that the thermal infrared pattern of an existing object blends into the background as if the object does not exist [8,9]. Meanwhile, various challenges arise accordingly in designing infrared illusion, which result mainly from complex surroundings, multifold heat-transfer modes, and fabrication difficulties.

Recent progress in infrared illusion focuses on two ways: regulating surface temperatures T_{sur} and designing surface emissivities ε_{sur}, which play two key roles in infrared imaging. On one hand, with the booming development of thermal metamaterials [10–17], temperature distributions can be tailored at will with elaborate microstructure designs. On this basis, thermal illusion has been achieved within fixed or varying backgrounds.

However, there are two weaknesses of this method in existing studies: firstly, most of them are confined to conductive systems [18–21], ignoring thermal convection and radiation; secondly, the surface structures are still identifiable from the background when viewed in visible light [22–24], which makes them hard conceal under multiband detection. On the other hand, tuning of emissivities can disguise an actual object as a fake one in an infrared camera. For self-adapting control, phase-change materials are widely used [25–28]. But these materials are not common, and usually call for additional installations to input a stimulus, adapting to changing circumstances (say, with changing temperatures). Besides, if ambient temperatures vary sharply or even out of the region of the phase-change temperature, its illusion effect will become invalid. So both of these methods of infrared illusion have some limitations. Furthermore, these two tailoring methods are mutually independent and scarcely coupled. This is due to the lack of a practical and synergistic platform.

To overcome the limitations and promote the integration of tuning of T_{sur} and ε_{sur} in a single platform, we design an omnithermal restructurable thermal metasurface for infrared illusion; see Fig. 1. By tailoring each block unit solely and assembling the blocks in a specific array, we can achieve characteristic infrared patterns. We consider the three modes of heat transfer, conduction, convection, and radiation (omnithermotics), which affect surface temperatures. With the radiation-cavity effect, say, the dependence of the effective emissivity on the sizes, shapes, and proportion of surface cavities, a specific emissivity can be achieved on each unit within a wide temperature range. Therefore, the surface temperature and emissivity can be
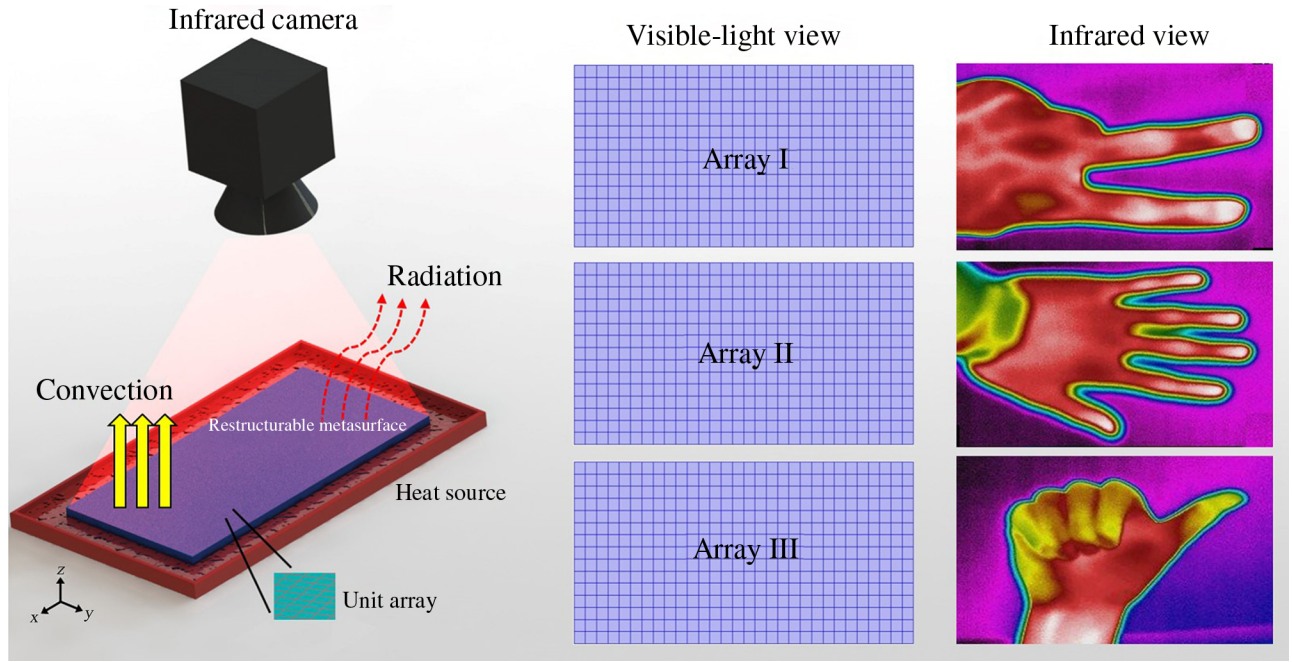
_____
[*]jphuang@fudan.edu.cn

FIG. 1. The proposed thermal metasurface. The units are arranged in three arrays (array I, array II, and array III), which can form three different images (specific gestures) in an infrared camera (right column). Meanwhile, they are similar when viewed in visible light (middle column).

tailored synergistically on this single platform. The unit-discretization operation in the x-y plane not only provides flexibility in designing fake temperature signals (hence yielding infrared illusion) but also makes different arrays almost identical (thus causing similarity in visible light) in spite of different properties (T_{sur} and ε_{sur}). As a result, both illusion for viewing in infrared light and similarity for viewing in visible light are achieved simultaneously, as schematically shown in the middle and right columns in Fig. 1.

II. THEORY

According to the Stefan-Boltzmann law [29], the total thermal radiative energy density I_{bb} of a black body is related to the fourth power of surface temperature T_{sur}:

$$I_{bb} = \int_0^\infty u_{bb}\,(\lambda,\,T_{sur})\,d\lambda = \int_0^\infty \frac{2\pi hc^2}{\lambda^5} \frac{1}{e^{\frac{hc}{\lambda k_B T_{sur}}} - 1}\,d\lambda$$

$$= \left(\frac{2\pi^5 k_B^4}{15c^2 h^3}\right) T_{sur}^4 = \sigma T_{sur}^4, \tag{1}$$

where λ is the radiative wavelength and $u_{bb}\,(\lambda,\,T_{sur})$ is the black-body spectral radiance, described by the Plank law. Here, h is the Plank constant, c is the velocity of light in a vacuum, k_B is the Boltzmann constant, and σ is the Stefan-Boltzmann constant. We consider the case where an infrared camera captures the infrared signals of an object in a far field for identification, where

the spectral radiance actually received deviates from the result described by Eq. (1). Spectral directional emissivity $\varepsilon_{sur}(\lambda,\,T_{sur},\theta,\phi)$ can describe this deviation, which is defined as the spectral-radiance ratio of actual objects to black bodies at temperature T_{sur}, wavelength λ, and direction angles θ and ϕ. But in most practical situations without elaborate directed thermal emission, the diffuse-emitter approximation is reasonable enough. So we can simplify the surface emissivity to $\varepsilon_{sur}(\lambda,\,T_{sur})$. Then the actual radiative energy density I_{ac} can be written as

$$I_{ac} = \int_0^\infty \varepsilon_{sur}\,(\lambda,\,T_{sur})\,u_{bb}\,(\lambda,\,T_{sur})\,d\lambda$$

$$= \int_0^\infty \varepsilon_{sur}\,(\lambda,\,T_{sur})\frac{2\pi hc^2}{\lambda^5}\frac{1}{e^{\frac{hc}{\lambda k_B T_{sur}}} - 1}\,d\lambda. \tag{2}$$

As we are concerned with the total thermal radiative energy instead of the spectral radiance, use of the full-wavelength emissivity $\varepsilon_{sur}(T_{sur})$ makes sense. It can be defined as

$$\varepsilon_{sur}(T_{sur}) = \frac{I_{ac}}{I_{bb}}$$

$$= \frac{\int_0^\infty \varepsilon_{sur}\,(\lambda,\,T_{sur})\,u_{bb}\,(\lambda,\,T_{sur})\,d\lambda}{\int_0^\infty u_{bb}\,(\lambda,\,T_{sur})\,d\lambda}$$

$$= \frac{\int_0^\infty \varepsilon_{sur}\,(\lambda,\,T_{sur})\,u_{bb}\,(\lambda,\,T_{sur})\,d\lambda}{\sigma T_{sur}^4}. \tag{3}$$

In addition to the fact that the intrinsic emissivity affects thermal radiation, both the signal-collection range and resolution of the infrared camera should also be considered. According to practical situation, the signal-collection range (λ_1, λ_2) covers the main emission band. Then the full-wavelength emissivity $\varepsilon_{\mathrm{sur}}(T_{\mathrm{sur}})$ can be used in this case. With use of Eqs. (2) and (3), the reading temperature T_{read} is given as [8]

$$
\begin{aligned}
T_{\mathrm{read}} &= CI_{\mathrm{ac}} = C \int_{\lambda_1}^{\lambda_2} \varepsilon_{\mathrm{sur}}(\lambda, T_{\mathrm{sur}}) u_{\mathrm{bb}}(\lambda, T_{\mathrm{sur}}) \, d\lambda \\
&\approx C\varepsilon_{\mathrm{sur}}(T_{\mathrm{sur}}) \int_{\lambda_1}^{\lambda_2} u_{\mathrm{bb}}(\lambda, T_{\mathrm{sur}}) \, d\lambda \\
&\approx C\varepsilon_{\mathrm{sur}}(T_{\mathrm{sur}}) \int_{\lambda_1}^{\lambda_2} \frac{2\pi h c^2}{\lambda^5} \frac{1}{e^{\frac{hc}{\lambda k_B T_{\mathrm{sur}}}} - 1} \, d\lambda,
\end{aligned} \tag{4}
$$

where C is a built-in conversion parameter of the infrared camera. Equation (4) indicates that two factors dominate the infrared imaging; namely, the camera capacity $[C, (\lambda_1, \lambda_2)]$ and the surface properties $(T_{\mathrm{sur}}, \varepsilon_{\mathrm{sur}})$. Here we focus on modulating the characteristic radiative spectrum, which depends on the surface properties $(T_{\mathrm{sur}}, \varepsilon_{\mathrm{sur}})$. Within a limited surface-temperature region, the full-wavelength emissivity $\varepsilon_{\mathrm{sur}}(T_{\mathrm{sur}})$ is regarded as $\varepsilon_{\mathrm{sur}}$, independent of T_{sur}. If the surface temperature varies sharply, the coupling relation between $\varepsilon_{\mathrm{sur}}$ and λ should considered. If the surface-temperature difference is large enough between units, the coupling relation between $\varepsilon_{\mathrm{sur}}$ and T_{sur} should also be taken into consideration. Our strategy for controllable infrared illusion consists in tuning T_{sur} and $\varepsilon_{\mathrm{sur}}$ individually and assembling them in any specific way.

For the first step, we consider a three-dimensional bulk as a unit, as illustrated in Fig. 2(a). We set its sides to be thermally insulated and place a homothermal source at the bottom. The heat flows in the bulk along the z axis and dissipates into the surroundings from the top surface due to convection and radiation. This process includes the three basic modes of heat transfer. In the steady state, the temperature of the top surface T_{sur} can be determined by the law of conservation of heat flow:

$$
\mathbf{J}_{\mathrm{cond}} = \mathbf{J}_{\mathrm{conv}} + \mathbf{J}_{\mathrm{rad}}, \tag{5}
$$

where $\mathbf{J}_{\mathrm{cond}}$, $\mathbf{J}_{\mathrm{conv}}$, and $\mathbf{J}_{\mathrm{rad}}$ are the conductive-heat-flow, convective-heat-flow and radiative-heat-flow density, respectively. We set the unit's height as H_b and thermal conductivity as κ_b. The convective coefficient and radiative emissivity of the surface are h_b and ε_b, respectively. The source and room temperatures are given as T_0 and T_{air}, respectively. We can write the expressions for $\mathbf{J}_{\mathrm{cond}}$, $\mathbf{J}_{\mathrm{conv}}$,
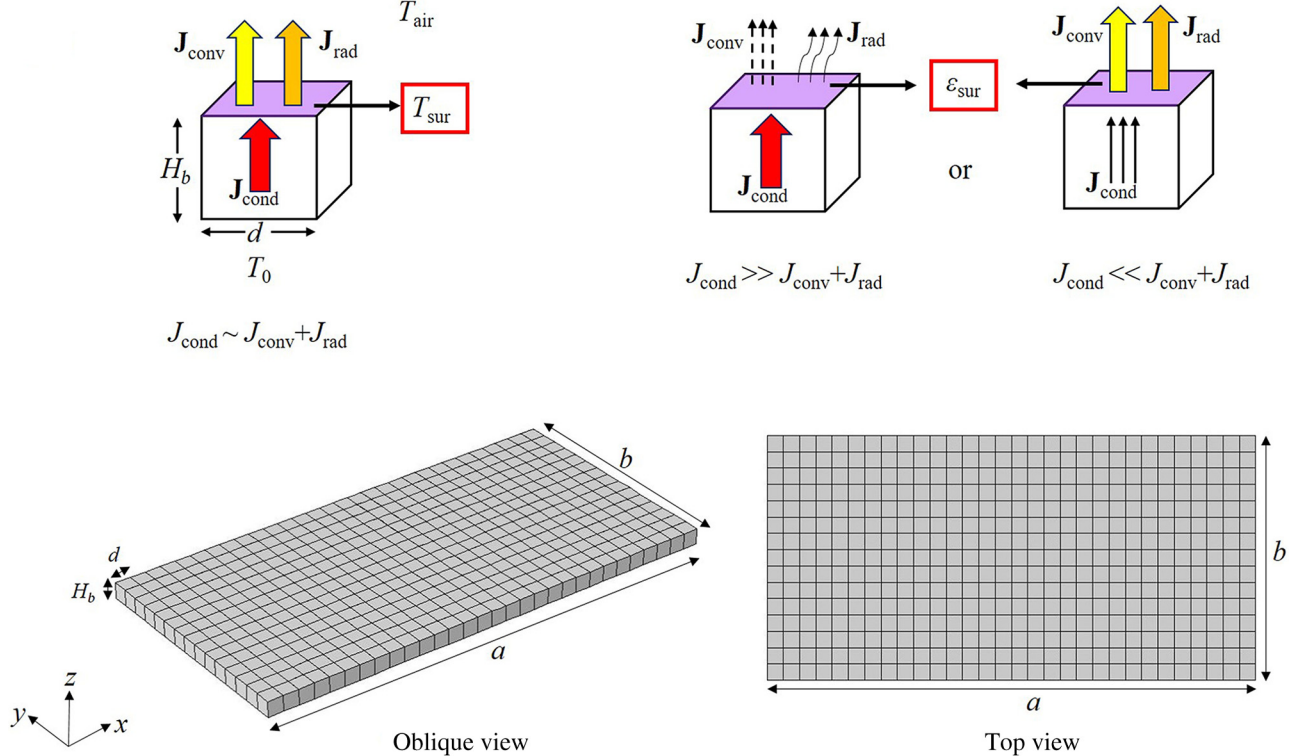

FIG. 2. Different tuning methods. (a),(b) A cuboid as a block unit. Conductive flow is comparable with convective and radiative flow in (a), but dramatically different in (b). (c) Assembly of the units, which form the whole metasurface.

and $\mathbf{J}_{\text{rad}}$ as

$$J_{\text{cond}} = \kappa_b \nabla T|_{\text{bulk}} = \kappa_b \frac{T_0 - T_{\text{sur}}}{H_b}, \tag{6a}$$

$$J_{\text{conv}} = h_b(T_{\text{sur}} - T_{\text{air}}), \tag{6b}$$

$$\begin{aligned} J_{\text{rad}} &= \varepsilon_b \sigma(T_{\text{sur}}^4 - T_{\text{air}}^4) \\ &= \varepsilon_b \sigma(T_{\text{sur}}^2 + T_{\text{air}}^2)(T_{\text{sur}} + T_{\text{air}})(T_{\text{sur}} - T_{\text{air}}) \\ &= R_b(T_{\text{sur}})(T_{\text{sur}} - T_{\text{air}}), \end{aligned} \tag{6c}$$

where $R_b(T) = \varepsilon_b \sigma(T_{\text{sur}}^2 + T_{\text{air}}^2)(T_{\text{sur}} + T_{\text{air}})$, representing the radiative ability of the surface. Combining Eqs. (5)–(6c), we can deduce the temperature of the top surface T_{sur} as

$$T_{\text{sur}} = \frac{\kappa_b T_0/H_b + [h_b + R_b(T_{\text{sur}})]\, T_{\text{air}}}{\kappa_b/H_b + h_b + R_b(T_{\text{sur}})}. \tag{7}$$

Here we obtain the general solution of the top-surface temperature of a unit. To obtain the value of T_{sur}, iteration of $R_b(T_{\text{sur}})$ should be performed with a calculator. Compared with the method reported in Ref. [18] where only κ_b is tuned, the present scheme has four free parameters. They are κ_b, h_b, ε_b, and H_b, involving the three basic modes of heat transfer. κ_b and H_b play roles in controlling conductive flow. h_b and ε_b correspond to convective and radiative flows, respectively. These four parameters can be expressed as

$$\kappa_b = \frac{H_b[h_b(T_{\text{sur}} - T_{\text{air}}) + \varepsilon_b \sigma(T_{\text{sur}}^4 - T_{\text{air}}^4)]}{T_0 - T_{\text{sur}}}, \tag{8a}$$

$$H_b = \frac{\kappa_b(T_0 - T_{\text{sur}})}{h_b(T_{\text{sur}} - T_{\text{air}}) + \varepsilon_b \sigma(T_{\text{sur}}^4 - T_{\text{air}}^4)}, \tag{8b}$$

$$h_b = \frac{\kappa_b(T_0 - T_{\text{sur}})/H_b - \varepsilon_b \sigma(T_{\text{sur}}^4 - T_{\text{air}}^4)}{T_{\text{sur}} - T_{\text{air}}}, \tag{8c}$$

$$\varepsilon_b = \frac{\kappa_b(T_0 - T_{\text{sur}})/H_b - h_b(T_{\text{sur}} - T_{\text{air}})}{\sigma(T_{\text{sur}}^4 - T_{\text{air}}^4)}. \tag{8d}$$

We can see if the surface temperature T_{sur} of each unit is preset to create a specific infrared illusion, only three of them are independent. Also, these four parameters can be tuned arbitrarily and simultaneously to achieve the designed T_{sur} of each unit. Thus, the tuning strategy is flexible. We suppose that ε_b (equivalent to ε_{sur}) is uniform in each unit and approximate it to that of a black body, and

then the reading temperature can be estimated by Eq. (4) as

$$T_{\text{read1}}(x, y) \approx C \int_{\lambda_1}^{\lambda_2} \frac{2\pi hc^2}{\lambda^5} \frac{1}{e^{\frac{hc}{\lambda k_B T_{\text{sur}}}} - 1} d\lambda \approx T_{\text{sur}}(x, y), \tag{9}$$

where (x, y) refers to the central position of each unit.

Tuning ε_b plays a limited role in controlling T_{sur} due to its maximum value of 1, especially in low-temperature regions. However, when T_{sur} is nearly uniform in each unit in some circumstances, tuning of the surface emissivity is another effective method for creating an illusion because ε_{sur} has a major impact beyond T_{sur} in Eq. (4). For example, according to Eq. (7), if κ_b is much greater than h_b and $R_b(T_{\text{sur}})$, T_{sur} will reach T_0. Inversely, it will reach T_{air}, as shown in Fig. 2(b). Then tailoring of the emissivity is the only way to create an infrared illusion in infrared imaging. On the basis of Eq. (4), the reading temperature in this case is

$$\begin{aligned} T_{\text{read2}}(x, y) &\approx \varepsilon_{\text{sur}}(x, y) \times C \int_{\lambda_1}^{\lambda_2} \frac{2\pi hc^2}{\lambda^5} \frac{1}{e^{hc/\lambda k_B T_{\text{sur}}} - 1} d\lambda \\ &\approx \varepsilon_{\text{sur}}(x, y) T_{\text{sur}}. \end{aligned} \tag{10}$$

The final step is to assemble these units in a specific array to create an infrared illusion in infrared imaging; see Fig. 2(c). Each unit can be regarded as a pixel. The fake surface temperature of each pixel should be distinguishable enough in infrared imaging so as to make the illusion valid. Therefore, the contrast ratio should be larger than the intrinsic resolution of the infrared camera under any conditions. The contrast ratio of imaging is based on the maximum and minimum values of the reading temperature. We can define the contrast ratio C as

$$C = \frac{T_{\text{read}}|_{\text{max}} - T_{\text{read}}|_{\text{min}}}{T_{\text{read}}|_{\text{max}} + T_{\text{read}}|_{\text{min}}}. \tag{11}$$

We have two ways for tailoring T_{read}. If the three modes of heat transfer are comparable, tuning T_{sur} solely is enough. According to Eq. (9), Eq. (11) can be written as

$$C_1 = \frac{T_{\text{sur}}|_{\text{max}} - T_{\text{sur}}|_{\text{min}}}{T_{\text{sur}}|_{\text{max}} + T_{\text{sur}}|_{\text{min}}}. \tag{12}$$

Otherwise, tuning ε_{sur} is necessary to give a distinguishable temperature distribution in the infrared camera. Substituting Eq. (10) into Eq. (11) yields the contrast ratio in this case as

$$C_2 = \frac{\varepsilon_{\text{sur}}|_{\text{max}} - \varepsilon_{\text{sur}}|_{\text{min}}}{\varepsilon_{\text{sur}}|_{\text{max}} + \varepsilon_{\text{sur}}|_{\text{min}}}. \tag{13}$$

The contrast ratio is related to the ratio of the surface temperature or the extremum difference of the effective

emissivity, representing an intrinsic character of a sort of specifically designed thermal metasurface. The flexible combination of units contributes to the reconfigurability and does not affect the contrast ratio C. So, once we design the units completely, the thermal metasurface will always meet the resolution requirement of the detector.

III. NUMERICAL SIMULATIONS

We perform finite-element simulations with the commercial software program COMSOL MULTIPHYSICS [30]. The simulations focus on tuning the temperature T_{sur}. Here we keep H_b fixed and tailor κ_b, h_b, and ε_b so as not to break the geometric construction of the metasurfaces. Firstly, the metasurface is constituted with 15×30 units, as shown in

Fig. 2(c). They are cubes of 1-cm length. Then we classify the total 450 units into six groups, as demonstrated in Fig. 3(a). Each group is designed independently so as to obtain six patterns of T_{sur}. Here we expect to create an illusion of "FUDAN." When tuning κ_b, we keep h_b and ε_b constant, and similarly for the other two parameters. Then the six groups are assembled as shown in Fig. 3(a). For simplification, we heat the entire lower surface with a homothermal heat source T_0 and keep the room temperature T_{air} at 300 K. The laterals of the surface are in thermal contact with neighboring units to mimic the real situation. Figures 3(b)–3(d), respectively, show the results of tuning κ_b, h_b, and ε_b at $T_0 = 350$ K, while Figs. 3(e)–3(g) show the results at $T_0 = 700$ K. We can see that convection and radiation play minor roles in low-temperature
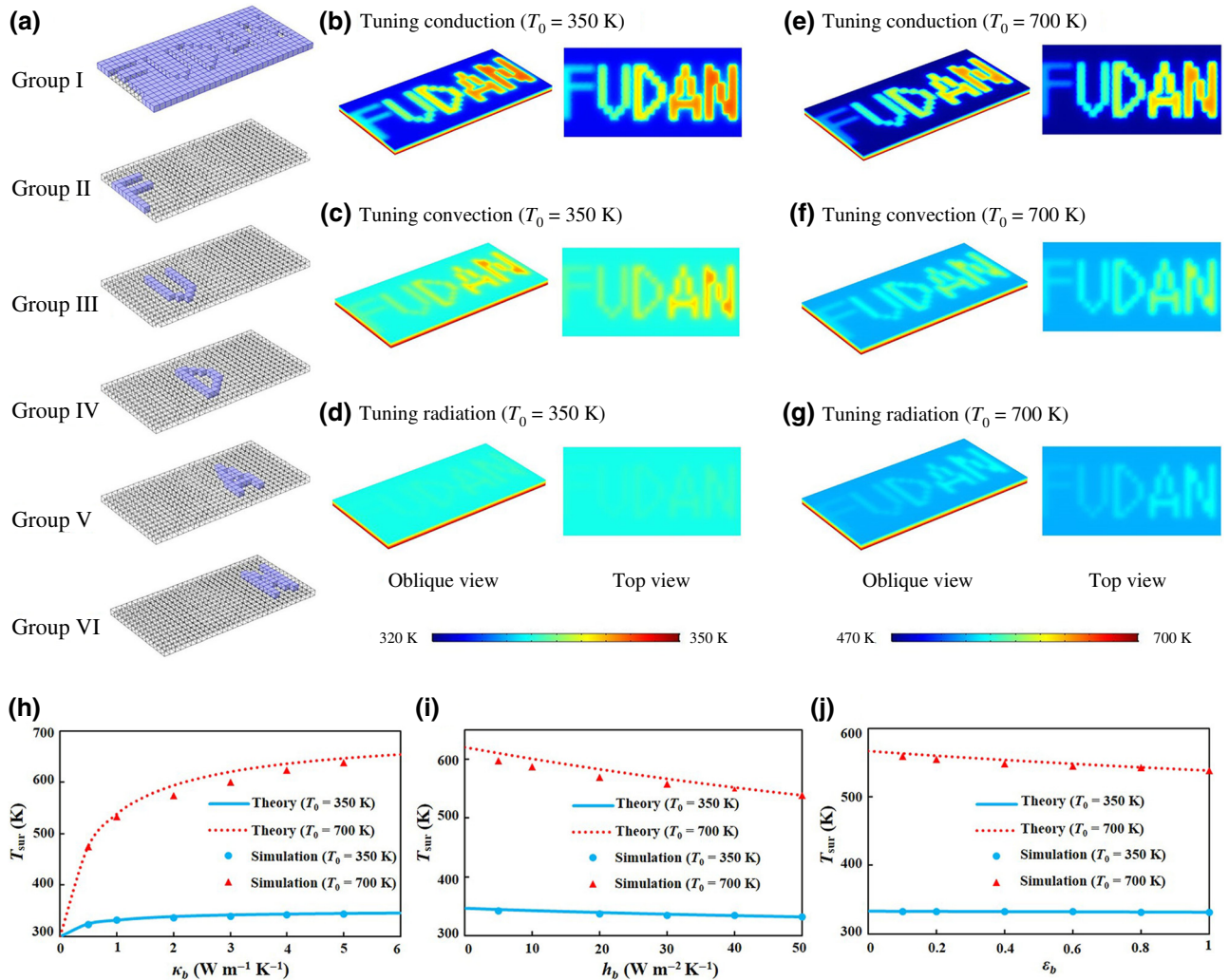

FIG. 3. Simulation results for tuning temperature T_{sur}. (a) Six groups and arrays with the letters "FUDAN." (b)–(g) Temperature distributions with different tuning methods. T_0 is set at 350 and 700 K. For tuning thermal conduction, κ_b is set as 0.5, 1, 2, 3, 4, and 5 W m^{-1} K^{-1} for the six groups, while h_b is 50 W m^{-2} K^{-1} and ε_b is 1. For tuning thermal convection, h_b is set at 5, 10, 20, 30, 40, and 50 W m^{-2} K^{-1}, while κ_b is 1 W m^{-1} K^{-1} and ε_b is 1. For tuning thermal radiation, ε_b is set at 0.1, 0.2, 0.4, 0.6, 0.8, and 1, while κ_b is 1 W m^{-1} K^{-1} and h_b is 50 W m^{-2} K^{-1}. (h)–(j) Comparisons between theoretical values and simulation values of T_{sur}, corresponding to the data extracted from (b)–(g).

surroundings. In particular, the effect of thermal radiation is nearly indistinguishable. When T_0 increases, the convection and radiation contribute to infrared patterns gradually. We calculate the contrast ratio C with the simulation data at 350 and 700 K. It is 2.96% and 15.23%, respectively, when we tune κ_b, and 0.20% and 2.28%, respectively, when we tune ε_b. Tuning ε_b has multiplicative effects when comparing with tuning κ_b, which confirms that radiation plays an increasingly important role with increasing temperature.

It is proved that by tuning the three heat-transfer modes individually, the expected patterns can be observed. Convection and radiation dominate at low and high temperatures, respectively, affecting the contrast ratio of the pattern in the infrared camera. Figures 3(h)–3(j) show comparisons of T_{sur} between theoretical data and simulation results under the three tuning modes. They show good agreement at low temperatures, and show a small shift when the temperature is high. This is because thermal interaction between different units starts to occur. More heat exchange in the x-y plane has an impact on T_{sur}. In extreme conditions (say, T_{sur} reaches T_0 or T_{air}), we have to tune the effective emissivity.

IV. EXPERIMENTAL VERIFICATION

As shown in Fig. 3(d), tuning radiation with emissivity at low temperature has little effect on infrared illusion. However, the engineered emissivities can impact the apparent-temperature distribution. Here we use the surface-cavity effect [31,32] to modulate $\varepsilon_{\mathrm{sur}}$. The cavity structures on the surface result in the block having higher radiant exitance. Hence, the apparent temperature in infrared imaging will deviate from the actual temperature, forming an illusive pattern. We are now in the position to design a surface-cavity structure. For simplification, we use a cylindrical structure as it is easy to manufacture, as demonstrated in Fig. 4(a). The heat transfer is between the surface cavity and free space, in which the angle factor of the cavity can be omitted. According to Ref. [31], the effective emissivity of an isolated cylindrical cavity ε_e depends on its area ratio of the mouth and the intracavity, which can be expressed as

$$\varepsilon_e = \left[1 + \frac{S_0}{S_1} \left(\frac{1}{\varepsilon_b} - 1 \right) \right]^{-1}, \tag{14}$$

where S_0 and S_1 are the areas of the mouth and the inwall, respectively, and $\varepsilon_{\mathrm{sur}}$ is the intrinsic surface emissivity. Owing to the high thermal conductivities and regular shape of the blocks, the surface temperature can be considered as a constant. The flat surface allows transfer of energy only into the environment, so thermal interaction occurs only between cavities. Thus, a quantitative emissivity expression for the whole surface of the block can be
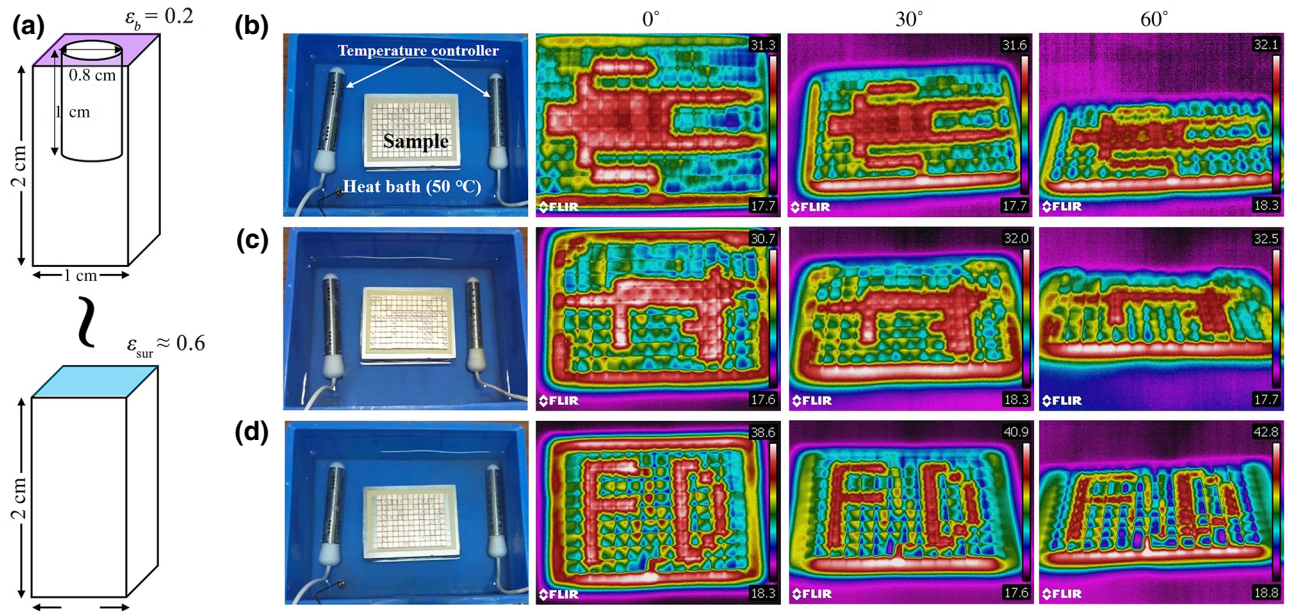

FIG. 4. Experimental measurements for different effective emissivities $\varepsilon_{\mathrm{sur}}$. (a) Cavity structure (upper panel) and effective-emissivity principle. The effective emissivity of a flat surface with a cavity (upper panel) is equivalent to $\varepsilon_{\mathrm{sur}}$ of another flat surface (lower panel), which is quantitatively expressed in Eqs. (14) and (15). The left image in (b)–(d) shows a photograph of the experimental apparatus for a human pattern, a machine-gun pattern, and an "FD" pattern, respectively. The three other images in (b)–(d) show the experimental measurements, each for one observation angle (0°, 30°, or 60°). The experimental apparatus is placed in a heat bath at 50 °C. The unit of the numerical values in the color bars is degree Celsius.

derived as

$$\varepsilon_{\text{sur}} = \varepsilon_e' \approx f\,\varepsilon_e + (1-f)\varepsilon_0$$
$$= f\left[1 + \frac{S_0}{S_1}\left(\frac{1}{\varepsilon_b} - 1\right)\right]^{-1} + (1-f)\varepsilon_b. \quad (15)$$

The area proportion of the cavity f (say, the area ratio of the mouth cavity to the whole surface) and the inherent area ratio S_0/S_1 enable us to tailor the effective emissivity of the surface so as to form a specific apparent-temperature distribution in infrared imaging.

We examine the practical effects directly with an FLIR E60 infrared camera, whose resolution is 0.1 K. For simplification, we use a 10×15 array and two groups of tailored units for designing feature patterns. Copper cubes 2 cm in length are used as block units. The thermal conductivity of copper is about $397\,\text{W}\,\text{m}^{-1}\,\text{K}^{-1}$, so that T_{sur} will approach the source temperature due to copper's good heat conduction. One group of units is not hollow with intrinsic emissivity 0.2, while the other has a cylindrical hole cut in it. The hole has a radius of 0.4 cm and a depth of 1 cm. According to Eq. (15), the effective emissivity is about 0.6. Besides, we design an acrylic plate with 15×20 square holes to encode the block units. They can be inserted in the holes for fixation. We design infrared patterns of a human, a machine gun, and the letters "FD," respectively, as shown in Figs. 4(b)–4(d), by manually rearranging these units. This operation can also be mechanically executed with additional active installations, thus forming an active restructurable metasurface. We place the encoded surface in a water bath, whose temperature is kept at 50 °C. The room temperature is about 20 °C. After the system reaches the steady state, the infrared camera helps to detect the feature patterns. The metasurfaces of different arrangements when viewed in visible light are hard to distinguish (similarity). At different observation angles, we find the robustness of illusion or similarity when viewed in infrared light or visible light respectively; see Figs. 4(b)–4(d). It is worth mentioning that when the surface is coated with an antireflection film, we find that the feature pattern disappears, and the reading temperatures become little higher than previously. This confirms that the cavity-engineering method helps to change the imaging.

V. DISCUSSION AND CONCLUSION

The emissivity and surface temperature of objects determine the imaging pattern of infrared cameras. Taking advantage of this, we demonstrate two methods of tuning emissivity and temperature by simulation or experiment on the same platform to achieve infrared-light illusion and visible-light similarity. Reference [18] gave a feasible implementation for tuning temperature by manipulating conduction processes. In addition to this, how to practically control convective and radiative flows needs

further study to satisfy theoretical predictions by Eqs. (8a)–(8d). Tuning T_{sur} works only with the system in the steady state, while tuning ε_{sur} works in both the steady state and a transient state. We note that the emissivity plays two roles in the tailoring process. On one hand, it guides the radiative flow so as to change the surface temperature. On the other hand, it helps conceal the real temperature T_{sur} to cheat the infrared camera and cause it to display an apparent temperature. So, we perform the variable-controlling method in the above-mentioned simulations and experiments. This platform is shown to be a flexible and applicable tool for infrared illusion. In different temperature regions, targeted tuning methods are available. Besides, the encoding and assembling process on unit cells is noninvasive and repeatable. Its flexibility with block assembly makes the illusion applicable to diverse situations. Moreover, infrared cameras usually have some limitation in dimensional resolution, and the illusion pattern quality can be improved when the sizes of the units are comparable with the dimensional resolution. The proposed restructurability is essentially distinguished with the common reconfigurability or adjustability [33]. This is because the former is property invariant but structurally rearrangeable, while the latter is structure invariant but property adjustable. The proposed restructurable metasurface exhibits both illusion in infrared light and similarity in visible light. The "similarity" can be upgraded to "indistinguishability" as long as the surface is structured carefully, as implied by Figs. 4(b)–4(d). This should be useful for real applications.

Also, as a direct application, we suggest to use our scheme to realize infrared anticounterfeiting. Anticounterfeiting is extensively applied in industry, the military, and daily life. The common strategies are based on optical holograms [34–36], which can be found by the naked eye or detectors. Nevertheless, such technologies tend to be defeated because the typical pattern can be forged. Recently, there has been much research on optical metasurfaces in this traditional field [37–40]. With carefully designed two-dimensional microstructures, the amplitude, phase, and polarization of light can be tailored arbitrarily. So, its intrinsic signal is characteristic and hard to replicate. However, as we need to capture only emissive electromagnetic-wave information for identification, an intuitional insight is to tailor the characteristic radiative signals for anticounterfeiting, which does not need additional incident light. The encryption process can be executed on our proposed metasurfaces, while decoding is achieved by infrared imaging. The key secret is hard to forge because of its similarity in visible light. Moreover, the restructurability raises the difficulty level for falsification. This kind of anticounterfeiting strategy has applicability in noninvasive and quick-recognition situations.

In summary, we propose a practical scheme for achieving infrared-light illusion and visible-light similarity. The

tuning of the surface temperature and emissivity can be executed synergistically. Compared with existing thermal metamaterials, our scheme considers all three basic modes of heat transfer (omnithermotics), thus expanding the scope of applications. Also, we introduce the cavity effect to tailor the emissivity, which simplifies the manufacture. We hope that this scheme can not only overcome some challenges in designing infrared illusion but that it also has direct applications in industry and commerce.

[1] D. G. Baranov, Y. Z. Xiao, I. A. Nechepurenko, A. Krasnok, A. Al, and M. A. Kats, Nanophotonic engineering of far-field thermal emitters, Nat. Mater. **18**, 920 (2019).

[2] J. C. Cuevas, Thermal radiation from subwavelength objects and the violation of Planck's law, Nat. Commu. **10**, 3342 (2019).

[3] W. Li and S. H. Fan, Nanophotonic control of thermal radiation for energy applications, Opt. Express **26**, 15995 (2018).

[4] S. M. Stewart, Spectral peaks and Wien's displacement law, J. Thermophys. Heat Transfer **26**, 689 (2012).

[5] X. He and L. Z. Wu, Illusion thermodynamics: A camouflage technique changing an object into another one with arbitrary cross section, Appl. Phys. Lett. **105**, 221904 (2014).

[6] R. Hu, S. L. Zhou, Y. Li, D.-Y. Lei, X. B. Luo, and C.-W. Qiu, Illusion thermotics, Adv. Mat. **30**, 1707237 (2018).

[7] F. B. Yang, L. J. Xu, and J. P. Huang, Thermal illusion of porous media with convection-diffusion process: Transparency, concentrating, and cloaking, ES Energy Environ. **6**, 45 (2019).

[8] Y. R. Qu, Q. Li, L. Cai, M. Y. Pan, P. Ghosh, K. K. Du, and M. Qiu, Thermal camouflage based on the phase-changing material GST, Light-Sci. Appl. **7**, 26 (2018).

[9] J. Shang, C. R. Jiang, L. J. Xu, and J. P. Huang, Many-particle thermal invisibility and diode from effective media, J. Heat Trans. **140**, 092004 (2018).

[10] C. Z. Fan, Y. Gao, and J. P. Huang, Shaped graded materials with an apparent negative thermal conductivity, Appl. Phys. Lett. **92**, 251907 (2008).

[11] T. Y. Chen, C.-N. Weng, and J.-S. Chen, Cloak for curvilinearly anisotropic media in conduction, Appl. Phys. Lett. **93**, 114103 (2008).

[12] S. Narayana and Y. Sato, Heat Flux Manipulation with Engineered Thermal Materials, Phys. Rev. Lett. **108**, 214303 (2012).

[13] T. C. Han, X. Bai, D. L. Gao, J. T. L. Thong, B. W. Li, and C.-W. Qiu, Experimental Demonstration of a Bilayer Thermal Cloak, Phys. Rev. Lett. **112**, 054302 (2014).

[14] Y. Li, X. Y. Shen, Z. H. Wu, J. Y. Huang, Y. X. Chen, Y. S. Ni, and J. P. Huang, Temperature-Dependent Transformation Thermotics: From Switchable Thermal Cloaks to Macroscopic Thermal Diodes, Phys. Rev. Lett. **115**, 195503 (2015).

[15] X. Y. Shen, Y. Li, C. R. Jiang, and J. P. Huang, Temperature Trapping: Energy-Free Maintenance of Constant Temperatures as Ambient Temperature Gradients Change, Phys. Rev. Lett. **117**, 055501 (2016).

[16] J. Wang, J. Shang, and J. P. Huang, Negative Energy Consumption of Thermostats at Ambient Temperature: Electricity Generation with Zero Energy Maintenance, Phys. Rev. Appl. **11**, 024053 (2019).

[17] L. J. Xu, S. Yang, and J. P. Huang, Passive Metashells with Adaptive Thermal Conductivities: Chameleonlike Behavior and its Origin, Phys. Rev. Appl. **11**, 054071 (2019).

[18] J. Shang, B. Y. Tian, C. R. Jiang, and J. P. Huang, Digital thermal metasurface with arbitrary infrared thermogram, Appl. Phys. Lett. **113**, 261902 (2018).

[19] R. Hu, S. Y. Huang, M. Wang, X. B. Luo, J. Shiomi, and C.-W. Qiu, Encrypted thermal printing with regionalization transformation, Adv. Mat. **31**, 1807849 (2019).

[20] T. Z. Yang, X. Bai, D. L. Gao, L. Z. Wu, B. W. Li, J. T. Thong, and C.-W. Qiu, Invisiable sensor: Simultaneous camouflaging and sensing in multiphysical fields, Adv. Mat. **27**, 7752 (2015).

[21] R. Hu, S. Y. Huang, M. Wang, L. L. Zhou, X. Y. Peng, and X. B. Luo, Binary Thermal Encoding by Energy Shielding and Harvesting Units, Phys. Rev. Appl. **10**, 054032 (2018).

[22] Y. Li, X. Bai, T. Z. Yang, H. L. Luo, and C.-W. Qiu, Structured thermal surface for radiative camouflage, Nat. Commun. **9**, 273 (2018).

[23] L. J. Xu, S. Yang, and J. P. Huang, Dipole-assisted thermotics: Experimental demonstration of dipole-driven thermal invisibility, Phys. Rev. E **100**, 062108 (2019).

[24] L. J. Xu, S. Yang, and J. P. Huang, Thermal illusion with the concept of equivalent thermal dipole, Eur. Phys. J. B **92**, 264 (2019).

[25] C. Y. Xu, G. T. Stiubianu, and A. A. Gorodetsky, Adaptive infrared-reflecting systems inspired by cephalopods, Science **359**, 1495 (2019).

[26] N. Lee, T. Kim, J.-S. Lim, I. Chang, and H. H. Cho, Metamaterial-selective emitter for maximizing infrared camouflage performance with energy dissipation, ACS Appl. Mater. Interfaces **11**, 21250 (2019).

[27] M. A. Kats, R. Blanchard, S. Y. Zhang, P. Genevet, C. Ko, S. Ramanathan, and F. Capasso, Vanadium Dioxide as a Natural Disordered Metamaterial: Perfect Thermal Emission and Large Broadband Negative Differential Thermal Emittance, Phys. Rev. X **3**, 041004 (2013).

[28] L. Xiao, H. Ma, J. K. Liu, W. Zhao, Y. Jia, Q. Zhao, K. Liu, Y. Wu, Y. Wei, S. S. Fan, and K. L. Jiang, Fast adaptive thermal camouflage based on flexible VO2/graphene/CNT thin films, Nano Lett. **15**, 8365 (2015).

[29] J. C. Cuevas and F. J. García-Vidal, Radiative heat transfer, ACS Photonics **5**, 3896 (2018).

[30] http://www.comsol.com/.

[31] Y. Ohwada, Calculation of the effective emissivity of a cavity having non-Lambertian isothermal surfaces, J. Opt. Soc. Am. A **16**, 1059 (1999).

[32] G. Mei, J. Zhang, S. Zhao, and Z. Xie, Simple method for calculating the local effective emissivity of the blackbody cavity as a temperature sensor, Infrared Phy. Tec. **85**, 372 (2017).

[33] L. Bao and T. J. Cui, Tunable, reconfigurable, and programmable metamaterials, Microw. Opt. Technol. Lett. **62**, 9 (2020).

[34] B. Javidi and J. L. Horner, Optical-pattern recognition for validation and security verification, Opt. Eng. **33**, 1752 (1994).

[35] X. S. Zhang, E. Dalsgaard, S. Liu, H. K. Lai, and J. Z. Chen, Concealed holographic coding for security applications lay using a moire technique, Appl. Opt. **36**, 8096 (1997).

[36] A. K. Aggarwal, S. K. Kaura, D. P. Chhachhia, and A. K. Sharma, Concealed moire pattern encoded security holograms readable by a key hologram, Opt. Laser Tech. **38**, 117 (2006).

[37] L. Huang, X. Chen, H. Mühlenbernd, H. Zhang, S. Chen, B. Bai, Q. Tan, G. Jin, K.-W. Cheah, C.-W. Qiu, J. Li, T. Zentgraf, and S. Zhang, Three-dimensional optical holography using a plasmonic metasurface, Nat. Commun. **4**, 2808 (2013).

[38] D. Wen, F. Yue, G. Li, G. Zheng, K. Chan, S. Chen, M. Chen, K. F. Li, P. W. H. Wong, K. W. Cheah, E. Y. B. Pun, S. Zhang, and X. Chen, Helicity multiplexed broadband metasurface holograms, Nat. Commun. **6**, 8241 (2015).

[39] C. M. Zhang, F. L. Dong, Y. Intaravanne, X. F. Zang, L. H. Xu, Z. W. Song, G. X. Zheng, W. Wang, W. G. Chu, and X. Z. Chen, Multichannel metasurfaces for anticounterfeiting, Phy. Rev. Appl. **12**, 034028 (2019).

[40] J. Sung, G.-V. Lee, and B. Lee, Progresses in the practical metasurface for holography and lens, Nanophotonics **8**, 1701 (2019).